

Non-Hermitian higher-order topological superconductors in two-dimension: statics and dynamics

Arnab Kumar Ghosh  ^{1, 2, *} and Tanay Nag  ^{3, †}

¹ Institute of Physics, Sachivalaya Marg, Bhubaneswar-751005, India

² Homi Bhabha National Institute, Training School Complex, Anushakti Nagar, Mumbai 400094, India

³ Department of Physics and Astronomy, Uppsala University, Box 516, 75120 Uppsala, Sweden

Being motivated by intriguing phenomena such as the breakdown of conventional bulk boundary correspondence and emergence of skin modes in the context of non-Hermitian (NH) topological insulators, we here propose a NH second-order topological superconductor (SOTSC) model that hosts Majorana zero modes (MZMs). Employing the non-Bloch form of NH Hamiltonian, we topologically characterize the above modes by biorthogonal nested polarization and resolve the apparent breakdown of the bulk boundary correspondence. Unlike the Hermitian SOTSC, we notice that the MZMs inhabit only one corner out of four in the two-dimensional NH SOTSC. We extend the static MZMs into the realm of Floquet drive. We find anomalous π -mode following low-frequency mass-kick in addition to the regular 0-mode that is usually engineered in a high-frequency regime. We further characterize the regular 0-mode with biorthogonal Floquet nested polarization. Our proposal is not limited to the d -wave superconductivity only and can be realized in the experiment with strongly correlated optical lattice platforms.

Introduction.— In recent times, topological phases in insulators and superconductors are extensively studied theoretically [1–6] as well as experimentally [7, 8]. The conventional bulk boundary correspondence (BBC) for first-order topological phase is generalized for $n(>1)$ th-order topological insulator (TI) [9–20] and topological superconductor [21–40] in $d \geq 2$ dimensions where there exist $n_c = (d - n)$ -dimensional boundary modes. The zero-dimensional (0D) corner and one-dimensional (1D) hinge modes are thus the hallmark signatures of higher-order topological insulator (HOTI) and higher-order topological superconductor (HOTSC). The dynamic analog of these phases are extensively studied for Floquet HOTI (FHOTI) [41–58] and Floquet HOTSC (FHOTSC) [59–65].

The realm of topological quantum matter is transcended from the Hermitian system to the non-Hermitian (NH) system due to the practical realization of TI phases in meta-materials [66–69] where energy conservation no longer holds [70, 71]. The NH description has a wide range of applications, including systems with source and drain [72, 73], in contact with the environment [74, 75], and involving quasiparticles of finite lifetime [76–78]. Apart from the complex eigenenergies and non-orthogonal eigenstates, the NH Hamiltonians uncover a plethora of intriguing phenomena in TI [71, 79–82] that do not have any Hermitian analog. For instance, NH Hamiltonian becomes non-diagonalizable at exceptional points (EPs) where eigenstates, corresponding to degenerate bands, coalesce [83, 84]; line and point are two different types of gaps in these systems that can be adiabatically transformed into a Hermitian and NH systems, respectively [80]; the conventional Bloch wave functions

do not precisely indicate the topological phase transitions under the open-boundary conditions (OBCs) leading to the breakdown of the BBC [85–91]; consequently, the non-Bloch-wave behavior results in the skin effect where the bulk states accumulate at the boundary [85–87], and the structure of topological invariants become intricate [79, 92–94].

While much has been explored on the HOTI phases in the context of NH systems [95–103], HOTSC counterpart, along with its dynamic signature, is yet to be examined. Note that NH 1D nanowire with s -wave pairing and p -wave SC chain are studied for the Majorana zero modes (MZMs) [104–109]. We, therefore, seek the answers to the following questions that have not been addressed so far-(a) How does the BBC change in HOTSC for the NH case as compared to the Hermitian case? (b) Can one use the concept of biorthogonal nested-Wilson-loop to characterize the MZMs there similar to that for HOT electronic modes [96]? (c) How can one engineer the anomalous FHOTSC phase for the NH case?

Considering the NH TI in the proximity to a d -wave superconductor, we illustrate the generation of the NH second-order topological superconductor (SOTSC). The breakdown of BBC is resolved with the non-Bloch nature of the NH Hamiltonian, where phase boundaries, obtained under different boundary conditions, become concurrent with each other (see Fig. 1). The SOTSC phase is characterized by the non-Bloch nested polarization. We demonstrate the NH skin effect where MZMs and bulk modes both display substantial corner localization (see Fig. 2). We further engineer the regular 0- and anomalous π -mode employing the mass-drive in high- and low-frequency regimes, respectively (see Figs. 4 and 5). We characterize the regular dynamic 0-mode by the non-Bloch Floquet nested polarization.

Realization of NH SOTSC.— We contemplate the following Hamiltonian of the NH SOTSC, consisting of NH TI $H_{\text{TI}}(\mathbf{k})$ and d -wave proximitized superconductivity

* arnob@iopb.res.in

† tanay.nag@physics.uu.se

[23, 63]

$$\mathcal{H}(\mathbf{k}) = \begin{pmatrix} H_{\text{TI}}(\mathbf{k}) - \mu & \Delta \\ \Delta^* & \mu - \tilde{H}_{\text{TI}}(-\mathbf{k}) \end{pmatrix}, \quad (1)$$

where, $\tilde{H}_{\text{TI}}(\mathbf{k}) = U_{\mathcal{T}}^{-1} H_{\text{TI}}^*(\mathbf{k}) U_{\mathcal{T}}$. Here, $H_{\text{TI}}(\mathbf{k}) = (\lambda_x \sin k_x + i\gamma_x) \sigma_x s_z + (\lambda_y \sin k_y + i\gamma_y) \sigma_y s_0 + (m_0 - t_x \cos k_x - t_y \cos k_y) \sigma_z s_0 = H_{\text{TI}}^H(\mathbf{k}) + i\gamma_x \sigma_x s_z + i\gamma_y \sigma_y s_0$, that preserves ramified (time-reversal symmetry) TRS: $U_{\mathcal{T}} \mathcal{H}_{\text{TI}}^*(\mathbf{k}) U_{\mathcal{T}}^{-1} = \mathcal{H}_{\text{TI}}(-\mathbf{k})$ and (particle-hole symmetry) PHS † : $U_{\mathcal{C}} \mathcal{H}_{\text{TI}}^*(\mathbf{k}) U_{\mathcal{C}}^{-1} = -\mathcal{H}_{\text{TI}}(-\mathbf{k})$ with $U_{\mathcal{T}} = \sigma_0 s_y$ and $U_{\mathcal{C}} = \sigma_x s_0$, respectively [80]. The d -wave superconducting paring is given by $\Delta(\mathbf{k}) = \Delta(\cos k_x - \cos k_y)$; whereas γ_x and γ_y introduce non-hermiticity in the Hamiltonian such that $H_{\text{TI}}(\mathbf{k}) \neq H_{\text{TI}}^{\dagger}(\mathbf{k})$. The hopping (spin-orbit coupling) amplitudes are given by $t_{x,y}$ ($\lambda_{x,y}$). Here, m_0 and μ account for the crystal field splitting and chemical potential, respectively. Notice that, $H_{\text{TI}}^H(\mathbf{k})$ respects TRS: $\mathcal{T} H_{\text{TI}}^H(\mathbf{k}) \mathcal{T}^{-1} = H_{\text{TI}}^H(-\mathbf{k})$ and PHS: $C H_{\text{TI}}^H(\mathbf{k}) \mathcal{C}^{-1} = -H_{\text{TI}}^H(-\mathbf{k})$; with $\mathcal{T} = iU_{\mathcal{T}}\mathcal{K}$ and $\mathcal{C} = U_{\mathcal{C}}\mathcal{K}$. The Hamiltonian (1) thus takes the following compact form $\mathcal{H}(\mathbf{k}) = \mathbf{N} \cdot \boldsymbol{\Gamma}$; where, $\mathbf{N} = \{\lambda_x \sin k_x + i\gamma_x, \lambda_y \sin k_y + i\gamma_y, m_0 - t_x \cos k_x - t_y \cos k_y, \Delta(\mathbf{k})\}$, $\boldsymbol{\Gamma} = \{\tau_z \sigma_x s_z, \tau_z \sigma_y s_0, \tau_z \sigma_z s_0, \tau_x \sigma_0 s_0\}$ with the Pauli matrices $\boldsymbol{\tau}$, $\boldsymbol{\sigma}$, and \mathbf{s} act on PH (e, h), orbital (α, β), and spin (\uparrow, \downarrow) degrees of freedom, respectively. Note that, $\mathcal{H}(\mathbf{k})$ obeys TRS and PHS † , generated by $\tilde{U}_{\mathcal{T}} = \tau_0 \sigma_0 s_y$ and $\tilde{U}_{\mathcal{C}} = \tau_y \sigma_0 s_y$, respectively.

The Hermitian system $\mathcal{H}^H(\mathbf{k})$ hosts zero-energy Majorana corner modes, protected by the TRS, in SOTSC phase for $m_0 < |t_x + t_y|$ while trivially gapped for $m_0 > |t_x + t_y|$ [23]. The NH system becomes defective at EPs provided $|E(\mathbf{k}_{\text{EP}})| = 0$ which is in a complete contrast to the Hermitian system with $E(\mathbf{k}) = 0$ at gapless point. A close inspection of Eq. (1) suggests that four-fold degenerate energy bands yield $|E(0, 0)| = 0$ [$|E(\pi, \pi)| = 0$] for $m_0^{+, \pm} = t_x + t_y \pm \sqrt{\gamma_x^2 + \gamma_y^2}$ [$m_0^{-, \pm} = -t_x - t_y \pm \sqrt{\gamma_x^2 + \gamma_y^2}$]. As a result, the gapless phase boundaries $m_0^s = s(t_x + t_y)$ for the Hermitian case are modified in the present NH case with $m_0^{s, \pm} = s(t_x + t_y) \pm \sqrt{\gamma_x^2 + \gamma_y^2}$; where, $s = \pm$ (see black lines in Figs. 1 (a)-(c)). This refers to the fact that $\text{Re}[E(\mathbf{k})]$ is gapless for $m_0^{s, -} < m_0 < m_0^{s, +}$ (see green-shaded region in Figs. 1 (a)-(c)). Furthermore, $\mathcal{H}(\mathbf{k})$ is expected to be gapped in real sector of energy for $m_0^{-, +} < m_0 < m_0^{+, -}$, hosting NH SOTSC phase.

The above conjecture, based on periodic boundary condition (PBC), is drastically modified when the NH system (1) is investigated under OBC. We show $|E|$, $\text{Re}[E]$ and $\text{Im}[E]$ under OBC with blue points in Figs. 1 (a), (b), and (c), respectively. Surprisingly, the MZMs continue to survive inside the green-shaded region i.e., beyond $m_0 = m_0^{-, +}$ and $m_0 = m_0^{+, -}$, till $m_0 < |\tilde{m}_0| = t_x + t_y + \gamma_x^2/2\lambda_x^2 + \gamma_y^2/2\lambda_y^2$, depicted by the red line, where the $\text{Re}[E]$ becomes gapless. All together this suggests the break-down of conventional BBC due to the non-Bloch nature of the NH Hamiltonian [85, 89–91]. This apparent

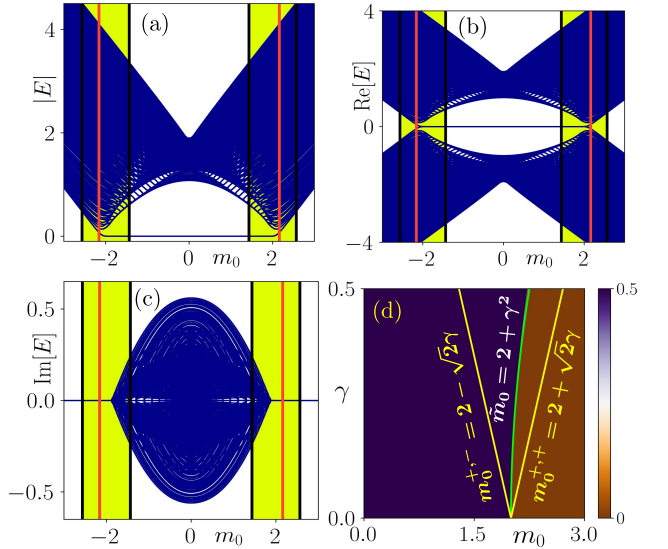


FIG. 1. We show $|E|$, $\text{Re}[E]$, and $\text{Im}[E]$, obtained from real space Hamiltonian under OBC in all directions using Eq. (1), as a function of m_0 in (a), (b), and (c), respectively. The mid-gap MZMs disappear into the bulk bands at $m_0 = \tilde{m}_0 = \pm(t_x + t_y + \gamma_x^2/2\lambda_x^2 + \gamma_y^2/2\lambda_y^2)$, defined by the red lines. The EPs $m_0^{s, \pm} = s(t_x + t_y) \pm \sqrt{\gamma_x^2 + \gamma_y^2}$ with $s = \pm$ are marked by black lines within which $\text{Re}[E(k)]$ associated with $\mathcal{H}(\mathbf{k})$ remains gapless as designated by green shaded region. (d) The topological phase diagram is depicted in the m_0 - γ plane using nested polarization $\langle \nu_{y, \mu'}^{\nu_x} \rangle$ Eq. (7). The yellow and green lines correspond to $m_0^{+, \pm}$ and \tilde{m}_0 , respectively while the latter separates SOTSC phase $\langle \nu_{y, \mu'}^{\nu_x} \rangle = 0.5$ from the trivial phase $\langle \nu_{y, \mu'}^{\nu_x} \rangle = 0.0$. The parameters used here are $t_x = t_y = \lambda_x = \lambda_y = \Delta = 1.0$ and $\gamma_x = \gamma_y = 0.4$.

ambiguity in BBC affects the calculation of topological invariants, which we investigate below.

Fig. 2 (a) demonstrates the complex-energy profile $\text{Im}[E]$ vs $\text{Re}[E]$ of Hamiltonian (1) in real space for $m_0 < |\tilde{m}_0|$. We find the line gap for the NH system irrespective of the boundary conditions as the complex-energy bands do not cross a reference line in the complex-energy plane. The origin, marked with red dot in Fig. 2 (a), indicates the MZMs under OBC that are further shown by the eight mid-gap states in $\text{Re}[E]$ - m (state index) plot (see Fig. 2 (b)). Analyzing the local density of states (LDOS) of the above MZMs, we find sharp localization only at one corner out of the four corners [95] (see Fig. 2 (c)). In addition, we remarkably find that the LDOS of the bulk modes also exhibits substantial corner localization as depicted in the insets of Fig. 2(c) [85–87]. The above features, reflecting the non-Block nature of the system, are referred to as the NH skin effect [85, 86]. This is in contrast to the Hermitian case where only the zero-energy modes can populate four corners of the 2D square lattice [13, 42, 46].

Topological characterization.— To this end, in order to compute the topological invariant from $\mathcal{H}(\mathbf{k})$ charac-

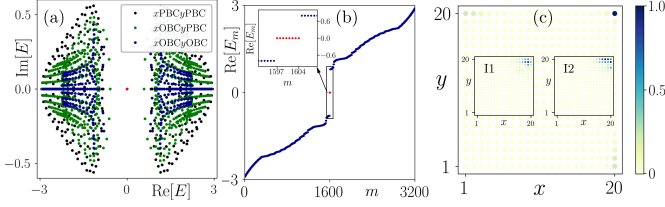


FIG. 2. (a) The eigenvalue spectrum for the real space 2D system Eq. (1), obeying PBC in both direction (black dots), PBC in y and OBC in x -direction (green dots), and OBC in both directions (blue dots) are depicted in complex energy plane. The zero-energy mode, obtained from OBC, is marked by red dots. (b) $\text{Re}[E_m]$ as a function of the state index m is displayed where eight mid-gap MZMs are highlighted in the inset. (c) The LDOS, associated with eight MZMs in (b), show sharp localization only at one corner. The LDOS for typical bulk states are shown in insets I1 (for $E_m = -2.631839$) and I2 (for $E_m = -1.738466 + 0.130006i$). We use $m_0 = 1.0$, while other parameters are same as Fig. 1.

terizing the SOTSC phase under OBC, we exploit the non-Bloch nature. We need to use the complex wave-vectors to describe open-boundary eigenstates such that $\mathbf{k} \rightarrow \mathbf{k}' + i\beta$ with $\beta_i = \gamma_i/\lambda_i$ ($i = x, y$) [79]. Upon replacing $k_{x,y} \rightarrow k'_{x,y} - i\gamma_{x,y}/\lambda_{x,y}$, the renormalized topological mass m'_0 acquires the following form in the limit $k_{x,y} \rightarrow 0$ and $\gamma_{x,y} \rightarrow 0$

$$m'_0 = m_0 - t_x - t_y - \frac{\gamma_x^2}{2\lambda_x^2} - \frac{\gamma_y^2}{2\lambda_y^2}. \quad (2)$$

Note that $|\tilde{m}_0| = |m'_0 - m_0|$ denotes phase boundary of the SOTSC phase as obtained from Fig. 1 (b). Employing $\mathbf{k}' \rightarrow \mathbf{k}'$ in $\mathcal{H}(\mathbf{k})$ i.e., $\mathcal{H}(\mathbf{k}) \rightarrow \mathcal{H}'(\mathbf{k}')$, we construct the Wilson loop operator as [10, 65]

$$W_{x,\mathbf{k}'} = F_{x,\mathbf{k}' + (L_x - 1)\Delta_x \mathbf{e}_x}(t) \cdots F_{x,\mathbf{k}' + \Delta_x \mathbf{e}_x} F_{x,\mathbf{k}'} \quad (3)$$

from the non-Bloch NH Hamiltonian $\mathcal{H}'(\mathbf{k}')$ [110, 111]. We define $[F_{x,\mathbf{k}'}]_{mn} = \langle \Psi_m^L(\mathbf{k}' + \Delta_x \mathbf{e}_x) | \Psi_n^R(\mathbf{k}') \rangle$, where $|\Psi_m^R(\mathbf{k}')\rangle$ ($\langle \Psi_m^L(\mathbf{k}') |$) represents the occupied right (left) eigenvectors of the Hamiltonian $\mathcal{H}'(\mathbf{k}')$ such that $\text{Re}[E'_m(\mathbf{k}')] < 0$; $\Delta_i = 2\pi/L_i$, with L_i being the the number of discrete points considered along i -th direction and \mathbf{e}_i being the unit vector along the said direction. Notice that, the bi-orthogonalization guarantees the following $\sum_n |\Psi_n^R(\mathbf{k}')\rangle \langle \Psi_m^L(\mathbf{k}')| = \mathbb{I}$ and $\langle \Psi_n^R(\mathbf{k}') | \Psi_n^R(\mathbf{k}') \rangle = \delta_{mn}$; where, n runs over all the energy levels irrespective of their occupations. The first-order polarization $\nu_{x,\mu}(k'_y)$ is obtained from the eigenvalue equation for $W_{x,\mathbf{k}'}$ as follows

$$W_{x,\mathbf{k}'} |\nu_{x,\mu}^R(\mathbf{k}')\rangle = e^{-2\pi i \nu_{x,\mu}(k'_y)} |\nu_{x,\mu}^R(\mathbf{k}')\rangle. \quad (4)$$

Note that unlike the Hermitian case, here $W_{x,\mathbf{k}'}$ is no longer unitary resulting in $\nu_{x,\mu}(k'_y)$ to be a complex number [96]. Importantly, $|\nu_{x,\mu}^R(\mathbf{k}')\rangle$ ($\langle \nu_{x,\mu}^L(\mathbf{k}') |$) designates bi-orthogonalized right (left) eigenvector of $W_{x,\mathbf{k}'}$ associated with $\mu = 1, \dots, 4$ -th eigenvalue. For a (second-order

topological) SOT system, the real part of first-order polarization exhibits a finite gap in spectra such that it can be divided into two sectors as $\pm \nu_x(k'_y)$ where each sector is two-fold degenerate. In order to characterize the SOT phase, we calculate the polarization along the perpendicular y -direction by projecting onto each $\pm \nu_x$ branch. This allows us to employ the nested Wilson loop as follows [10, 65]

$$W_{y,\mathbf{k}'}^{\pm \nu_x} = F_{y,\mathbf{k}' + (L_y - 1)\Delta_y \mathbf{e}_y}^{\pm \nu_x} \cdots F_{y,\mathbf{k}' + \Delta_y \mathbf{e}_y}^{\pm \nu_x} F_{y,\mathbf{k}'}^{\pm \nu_x}. \quad (5)$$

Here, $[F_{y,\mathbf{k}'}^{\pm \nu_x}]_{\mu_1 \mu_2} = \sum_{mn} [\nu_{x,\mu_1}^L(\mathbf{k}' + \Delta_y \mathbf{e}_y)]_m^* [F_{y,\mathbf{k}'}]_{mn} [\nu_{x,\mu_2}^R(\mathbf{k}')]_n$ with $[F_{y,\mathbf{k}'}]_{mn} = \langle \Psi_m^L(\mathbf{k}' + \Delta_y \mathbf{e}_y) | \Psi_n^R(\mathbf{k}') \rangle$. The indices $\mu_{1,2} \in \pm \nu_x$ run over the projected eigenvectors of $W_{x,\mathbf{k}'}$ only. We evaluate $W_{y,\mathbf{k}'}^{\pm \nu_x}$ for a given value of k'_x that is the base point while calculating $W_{x,\mathbf{k}'}$ (3).

The nested polarization $\nu_{y,\mu'}^{\pm \nu_x}(k'_x)$ can be extracted by solving the eigenvalue equation for $W_{y,\mathbf{k}'}$

$$W_{y,\mathbf{k}'}^{\pm \nu_x} |\nu_{y,\mu'}^{\pm \nu_x}(\mathbf{k}')\rangle = e^{-2\pi i \nu_{y,\mu'}^{\pm \nu_x}(k'_x)} |\nu_{y,\mu'}^{\pm \nu_x}(\mathbf{k}')\rangle. \quad (6)$$

The average nested Wannier sector polarization $\langle \nu_{y,\mu'}^{\pm \nu_x} \rangle$ for the μ' -th branch, characterizing the 2D SOTSC, is given by

$$\langle \nu_{y,\mu'}^{\pm \nu_x} \rangle = \frac{1}{L_x} \sum_{k'_x} \text{Re} [\nu_{y,\mu'}^{\pm \nu_x}(k'_x)]. \quad (7)$$

We explore the SOT phase diagram by investigating $\text{mod}(\langle \nu_{y,\mu'}^{\pm \nu_x} \rangle, 1.0)$ in the m_0 - γ ($\gamma_x = \gamma_y = \gamma$) plane keeping $t_x = t_y = \lambda_x = \lambda_y = 1$ (see Fig. 1(d)). The blue (brown) region indicates the SOTSC and trivial phase. The green line in Fig. 1 (d), separating the above two phases, represents the phase boundary $\tilde{m}_0 = 2 + \gamma^2$ as demonstrated in Eq. (2). On the other hand, the phase boundaries, obtained from bulk Hamiltonian (1), are found to be $m_0^{\pm, \pm} = 2 \pm \sqrt{2}\gamma$ that are depicted by yellow lines in Fig. 1 (d). Therefore, the topological invariant, computed using the non-Bloch Hamiltonian $\mathcal{H}'(\mathbf{k}')$, can accurately predict the MZMs as obtained from the real space Hamiltonian under OBC (see Fig. 1 (c)). This correspondence for very higher values of γ no longer remains appropriate due to the possible break down of Eq. (2).

s-wave NH SOTSC.— The above discussions of NH HOTSC is not limited to the *d*-wave superconductivity and can be contemplated for *s*-wave superconductivity with pairing amplitude Δ_s as follows [28, 62] $\mathcal{H}(\mathbf{k}) = \mathbf{N} \cdot \boldsymbol{\Gamma}$; where, $\mathbf{N} = \{\lambda_x \sin k_x + i\gamma_x, \lambda_y \sin k_y + i\gamma_y, m_0 - t_x \cos k_x - t_y \cos k_y, \Delta_s, \Lambda(\cos k_x - \cos k_y)\}$, $\boldsymbol{\Gamma} = \{\tau_z \sigma_x s_z, \tau_z \sigma_y s_0, \tau_z \sigma_z s_0, \tau_x \sigma_0 s_0, \tau_0 \sigma_x s_x\}$. The last term proportional to Λ represents C_4 symmetry breaking Wilson-Dirac mass term. We depict the corresponding complex-energy bands in complex energy plane, eigenvalue spectra highlighting the mid-gap states, and the LDOS associated to the MZMs and bulk modes in Fig. 3 (a), (b), and (c), respectively. The NH SOTSC phase

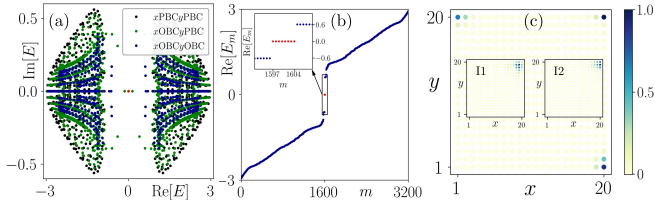


FIG. 3. We repeat Fig. 2 for s -wave pairing case with $\Delta_s = 0.4$ and $\Lambda = 1.0$. We choose $E_m = -2.666466$ and $E_m = -1.713832 + 0.038500i$ for insets I1 and I2 in (c), respectively. All the remaining parameters are same as Fig. 1.

with Δ_s can also be obtained using in-plane magnetic field instead of C_4 symmetry breaking [30, 62]. The topological characterization of these phases we leave for future studies.

Floquet generation of NH SOTSC.— Having studied the static NH SOTSC, we seek the answer to engineer dynamic NH SOTSC out of trivial phase by periodically kicking the on-site mass term of the Hamiltonian $\mathcal{H}(\mathbf{k})$ (Eq. (1)) as [56, 63]

$$m(t) = m_1 \sum_{r=-\infty}^{\infty} \delta(t - rT) . \quad (8)$$

Here, m_1 and T represent the strength of the drive and the time-period, respectively. The Floquet operator is formulated to be

$$\begin{aligned} U(\mathbf{k}, T) &= \text{TO} \exp \left[-i \int_0^T dt \{ \mathcal{H}(\mathbf{k}) + m(t) \Gamma_3 \} \right] \\ &= \exp[-i\mathcal{H}(\mathbf{k})T] \exp[-im_1\Gamma_1] , \end{aligned} \quad (9)$$

where TO denotes the time ordering. Notice that $m_0 > |t_x + t_y + \sqrt{\gamma_x^2 + \gamma_y^2}|$ such that the underlying static NH Hamiltonian $\mathcal{H}(\mathbf{k})$ remains in the trivially gapped phase. Having constructed the Floquet operator $U(\mathbf{k}, T)$, we resort to OBCs and diagonalize the Floquet operator to obtain the quasi-energy spectrum for the system. We depict the real part of the quasi-energy μ_m as function of the state index m in Fig. 4 (a) where frequency of the drive is higher than the band-width of the system. The existence of eight MZMs is a signature of the NH Floquet SOTSC phase. The LDOS for the MZMs displays substantial localization only at one corner in Fig. 4(b). Insets show the NH skin effect where the bulk modes at finite energy also have a fair amount of corner localization.

In order to topologically characterize the above MZMs, we again make use of the non-Bloch form. Instead of the static Hamiltonian, we derive the high-frequency effective Floquet Hamiltonian, in the limit $T \rightarrow 0$ and $m_1 \rightarrow 0$ to analyze the situation

$$H_{\text{Flq}}(\mathbf{k}) \approx \mathcal{H}(\mathbf{k}) + \frac{m_1}{T} \Gamma_1 + m_1 \sum_{j=2}^4 N_j \Gamma_{j1} , \quad (10)$$

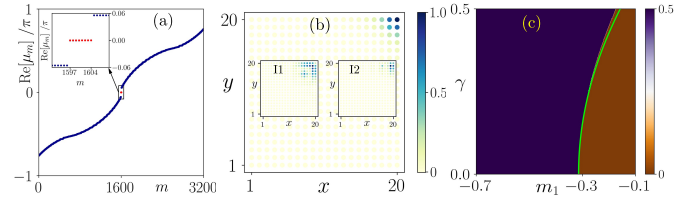


FIG. 4. (a) The real part of the quasi-energy spectrum E_m , obtained from Eq. (9) under OBC, are shown with eight Floquet Majorana 0-modes in the inset. (b) The LDOS, associated with eight MZMs in (a), exhibits substantial localization only at one corner similar to Fig. 2 (c). The LDOS for typical bulk modes with $E_m = -0.697702\pi$ and -0.453177π are demonstrated in insets I1 and I2. (c) The topological phase diagram is depicted in the m_1 - γ plane where the Floquet SOTSC phase is characterized by the average Floquet nested Wannier sector polarization $\langle \nu_{y,\mu'}^{\text{F},\nu_x} \rangle = 0.5$ (blue region). The phase boundary, marked by green line, is consistent with Eq. (11). We consider $m_0 = 2.5$, $m_1 = -0.4$, $\Omega = 10.0$ such that we start from the trivial phase deep inside the brown region in Fig. 1 (c).

with $\Gamma_{21} = -\sigma_y s_z$, $\Gamma_{31} = \sigma_x$, $\Gamma_{41} = -\tau_y \sigma_z$. Upon substitution of $\mathbf{k} \rightarrow \mathbf{k}' + i\beta$, the modified mass term in $H'_{\text{Flq}}(\mathbf{k}')$ reads as

$$m'_0 = m_0 - t_x - t_y - \frac{\gamma_x^2}{2\lambda_x^2} - \frac{\gamma_y^2}{2\lambda_y^2} + \frac{m_1}{T} . \quad (11)$$

Evaluating the effective Floquet nested Wannier sector polarization $\langle \nu_{y,\mu'}^{\text{F},\pm\nu_x} \rangle$ numerically from non-Bloch Floquet operator $U'(\mathbf{k}', T)$ [47, 65], we obtain the Floquet phase diagram in m_1 - γ plane as shown in Fig. 4 (c). The non-Bloch Floquet operator can be considered as the dynamic analog of the non-Bloch NH Hamiltonian $H'(\mathbf{k}')$. In particular, we use bi-orthogonalized $|\Psi_{\text{F}}^{\text{R}}(\mathbf{k}')\rangle$ ($\langle\Psi_{\text{F}}^{\text{L}}(\mathbf{k}')|$), representing the occupied right (left) quasi-states of $U'(\mathbf{k}', T)$ with quasi-energy $-\pi/T < \text{Re}[\mu] < 0$, to construct the Wilson loops $W_{x,\mathbf{k}'}^{\text{F}}$ for the driven case. Following identical line of arguments, presented for the static case, $W_{y,\mathbf{k}'}^{\text{F},\pm\nu_x}$ is obtained from $\left[F_{y,\mathbf{k}'}^{\text{F},\pm\nu_x} \right]_{\mu_1 \mu_2} = \sum_{mn} \left[\nu_{x,\mu_1}^{\text{F},\text{L}}(\mathbf{k}' + \Delta_y \mathbf{e}_y) \right]_m^* \left[F_{y,\mathbf{k}'}^{\text{F}} \right]_{mn} \left[\nu_{x,\mu_2}^{\text{F},\text{R}}(\mathbf{k}') \right]_n$ with $\left[F_{y,\mathbf{k}'}^{\text{F}} \right]_{mn} = \langle \Psi_{\text{F}}^{\text{L}}(\mathbf{k}' + \Delta_y \mathbf{e}_y) | \Psi_{\text{F}}^{\text{R}}(\mathbf{k}') \rangle$ and $|\nu_{x,\mu}^{\text{F},\text{R}}(\mathbf{k}')\rangle$ ($\langle \nu_{x,\mu}^{\text{F},\text{L}}(\mathbf{k}') |$) designates bi-orthogonalized right (left) eigenvector of $W_{x,\mathbf{k}'}^{\text{F}}$. Interestingly, this is similar to the static phase diagram where the phase boundary is accurately explained by Eq. (11).

We further analyze the problem for lower frequency regime to look for anomalous Floquet modes at quasienergy $\text{Re}[\mu] = \pm\pi$ [56, 65]. We depict one such scenario for $\Omega = 2\pi/T = 5.0$ in Fig. 5 (a) where eight anomalous π -modes appear simultaneously with regular eight 0-modes. The corresponding LDOS for 0-mode and π -mode are shown in Fig. 5(b) and (c), respectively. Interestingly, the 0-mode and the π -mode populate different corners of the system. As a signature of NH skin

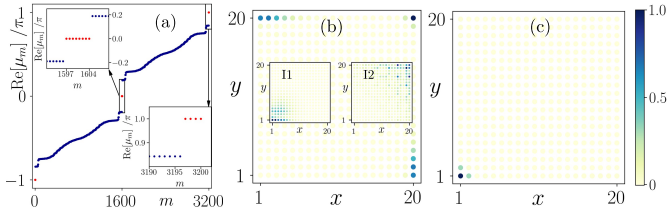


FIG. 5. (a) We repeat Fig. 4 (a) considering the low frequency mass-kick with $\Omega = 5.0$ where we find eight regular 0- and anomalous π -modes simultaneously. We show the LDOS associated with $\text{Re}[E_m] = 0$ - and $\text{Re}[E_m] = +\pi$ in (b) and (c), respectively. The LDOS for Floquet bulk modes with $E_m = -0.838779\pi - 0.085397\pi i$ and -0.471932π are respectively depicted in the insets I1 and I2 of (b). We consider $m_0 = 0, m_1 = 1.5, \Omega = 5.0$.

effect, we show the LDOS for two bulk states in the inset I1 and I2 of Fig. 5(b). The localization profile of the zero-energy states and bulk states are unique to the NH system that we leave here for further future studies.

Discussions.— It has been shown for NH HOTI phases that zero modes, localized on a single corner, are protected by the mirror-rotation and sub-lattice symmetries [95]. The above symmetries play crucial role for the single corner localization of MZMs in our case. The non-Bloch version of nested bulk polarization is relied on the mirror symmetry of the underlying Hermitian Hamiltonian [65]. The number of MZMs can be tuned in our case by the application of magnetic field similar to the Hermitian SOTSC phase [63]. Interestingly, Hermitian and non-Hermitian phases belong to the Dirac and non-Hermitian Dirac universality classes [112, 113]. In the case of HOT phases, one expects different critical exponents with respect to the usual Dirac model. The breakdown of BBC and skin effect are intimately related to such non-Hermitian Dirac universality class. The edge theory, computed from Hermitian HOT model, is modified due to the non-Hermiticity with the possible non-

Bloch form. Coming to experimental relevance, we believe that the optical lattice can be considered to be an experimentally viable platform to execute the theoretical proposals on NH systems [73, 114, 115].

Summary and conclusions.— In this article, we consider 2D NH TI, proximized with d -wave superconductivity, to investigate the emergence of NH SOTSC phase. From the analysis of EPs on the bulk NH Hamiltonian under PBC, one can estimate the gapped and gapless phase in terms of the real energies (see Fig. 1). By contrast, the MZMs, obtained from the real space NH Hamiltonian under OBC, do not immediately vanish inside the bulk gapless region (see Fig. 2). This apparent breakdown of the BBC can be explained by the non-Bloch nature of the NH Hamiltonian that further results in the MZMs residing at only one corner while the bulk modes populate the boundaries. While the later is dubbed as NH skin effect. We propose the nested polarization for topologically characterize the MZMs upon exploiting the non-Bloch form of the complex wave vectors. This resolves the anomaly between the phase boundaries, obtained from OBC and PBC, in the topological phase diagram. Finally, we adopt a mass-kick drive to illustrate the Floquet generation of NH SOTSC out of the trivial phase and characterize it using non-Bloch Floquet nested Wannier sector polarization (see Fig. 4). In addition, we demonstrate the emergence of anomalous π -mode following such drive when the frequency is lowered (see Fig. 5). However, the characterization of these anomalous π -modes is beyond the scope of the present study that we leave for future studies [47, 65]. The disorder analog of NH HOT phases can also be further explored in future.

Acknowledgments.— A.K.G. acknowledges SAMKHYA: High-Performance Computing Facility provided by Institute of Physics, Bhubaneswar, for numerical computations. We thank Arijit Saha for useful discussions. We have used the Julia programming language [116] for our numerical computations.

-
- [1] M. Z. Hasan and C. L. Kane, “Colloquium: topological insulators,” *Rev. Mod. Phys.* **82**, 3045 (2010).
- [2] F. D. M. Haldane, “Model for a quantum hall effect without landau levels: Condensed-matter realization of the ‘parity anomaly’,” *Phys. Rev. Lett.* **61**, 2015–2018 (1988).
- [3] C. L. Kane and E. J. Mele, “ Z_2 topological order and the quantum spin hall effect,” *Phys. Rev. Lett.* **95**, 146802 (2005).
- [4] B. A. Bernevig, T. L. Hughes, and S.-C. Zhang, “Quantum spin hall effect and topological phase transition in hgte quantum wells,” *Science* **314**, 1757–1761 (2006).
- [5] J. Alicea, “New directions in the pursuit of majorana fermions in solid state systems,” *Rep. Prog. Phys.* **75**, 076501 (2012).
- [6] C. Beenakker, “Search for majorana fermions in superconductors,” *Annu. Rev. Condens. Matter Phys.* **4**, 113–136 (2013).
- [7] G. Jotzu, M. Messer, R. Desbuquois, M. Lebrat, T. Uehlinger, D. Greif, and T. Esslinger, “Experimental realization of the topological haldane model with ultracold fermions,” *Nature* **515**, 237–240 (2014).
- [8] A. Das, Y. Ronen, Y. Most, Y. Oreg, M. Heiblum, and H. Shtrikman, “Zero-bias peaks and splitting in an alinas nanowire topological superconductor as a signature of majorana fermions,” *Nat. Phys.* **8**, 887–895 (2012).
- [9] W. A. Benalcazar, B. A. Bernevig, and T. L. Hughes, “Quantized electric multipole insulators,” *Science* **357**, 61–66 (2017).
- [10] W. A. Benalcazar, B. A. Bernevig, and T. L. Hughes, “Electric multipole moments, topological multipole moment pumping, and chiral hinge states in crystalline insulators,” *Phys. Rev. B* **96**, 245115 (2017).
- [11] Z. Song, Z. Fang, and C. Fang, “($d - 2$)-dimensional

- edge states of rotation symmetry protected topological states,” *Phys. Rev. Lett.* **119**, 246402 (2017).
- [12] J. Langbehn, Y. Peng, L. Trifunovic, F. von Oppen, and P. W. Brouwer, “Reflection-symmetric second-order topological insulators and superconductors,” *Phys. Rev. Lett.* **119**, 246401 (2017).
- [13] F. Schindler, A. M. Cook, M. G. Vergniory, Z. Wang, S. S. Parkin, B. A. Bernevig, and T. Neupert, “Higher-order topological insulators,” *Science adv.* **4**, eaat0346 (2018).
- [14] S. Franca, J. van den Brink, and I. C. Fulga, “An anomalous higher-order topological insulator,” *Phys. Rev. B* **98**, 201114 (2018).
- [15] Z. Wang, B. J. Wieder, J. Li, B. Yan, and B. A. Bernevig, “Higher-order topology, monopole nodal lines, and the origin of large fermi arcs in transition metal dichalcogenides xte_2 ($x = Mo, W$),” *Phys. Rev. Lett.* **123**, 186401 (2019).
- [16] D. Călugăru, V. Jurićić, and B. Roy, “Higher-order topological phases: A general principle of construction,” *Phys. Rev. B* **99**, 041301 (2019).
- [17] P. Szumniak, D. Loss, and J. Klinovaja, “Hinge modes and surface states in second-order topological three-dimensional quantum hall systems induced by charge density modulation,” *Phys. Rev. B* **102**, 125126 (2020).
- [18] X. Ni, M. Li, M. Weiner, A. Alù, and A. B. Khanikaev, “Demonstration of a quantized acoustic octupole topological insulator,” *Nature Communications* **11**, 2108 (2020).
- [19] B. Xie, H. Wang, X. Zhang, P. Zhan, J. Jiang, M. Lu, and Y. Chen, “Higher-order band topology,” *Nat. Rev. Phys.* **3**, 520–532 (2021).
- [20] S. Saha, T. Nag, and S. Mandal, “Dipolar quantum spin hall insulator phase in extended haldane model,” (2022), [arXiv:2204.06641](https://arxiv.org/abs/2204.06641).
- [21] X. Zhu, “Tunable majorana corner states in a two-dimensional second-order topological superconductor induced by magnetic fields,” *Phys. Rev. B* **97**, 205134 (2018).
- [22] T. Liu, J. J. He, and F. Nori, “Majorana corner states in a two-dimensional magnetic topological insulator on a high-temperature superconductor,” *Phys. Rev. B* **98**, 245413 (2018).
- [23] Z. Yan, F. Song, and Z. Wang, “Majorana corner modes in a high-temperature platform,” *Phys. Rev. Lett.* **121**, 096803 (2018).
- [24] Y. Wang, M. Lin, and T. L. Hughes, “Weak-pairing higher order topological superconductors,” *Phys. Rev. B* **98**, 165144 (2018).
- [25] R.-X. Zhang, W. S. Cole, and S. Das Sarma, “Helical hinge majorana modes in iron-based superconductors,” *Phys. Rev. Lett.* **122**, 187001 (2019).
- [26] R.-X. Zhang, W. S. Cole, X. Wu, and S. Das Sarma, “Higher-order topology and nodal topological superconductivity in fe(se,te) heterostructures,” *Phys. Rev. Lett.* **123**, 167001 (2019).
- [27] Y. Volpez, D. Loss, and J. Klinovaja, “Second-order topological superconductivity in π -junction rashba layers,” *Phys. Rev. Lett.* **122**, 126402 (2019).
- [28] Z. Yan, “Majorana corner and hinge modes in second-order topological insulator/superconductor heterostructures,” *Phys. Rev. B* **100**, 205406 (2019).
- [29] S. A. A. Ghorashi, X. Hu, T. L. Hughes, and E. Rossi, “Second-order dirac superconductors and magnetic field induced majorana hinge modes,” *Phys. Rev. B* **100**, 020509 (2019).
- [30] Y.-J. Wu, J. Hou, Y.-M. Li, X.-W. Luo, X. Shi, and C. Zhang, “In-plane zeeman-field-induced majorana corner and hinge modes in an s -wave superconductor heterostructure,” *Phys. Rev. Lett.* **124**, 227001 (2020).
- [31] K. Laubscher, D. Chughtai, D. Loss, and J. Klinovaja, “Kramers pairs of majorana corner states in a topological insulator bilayer,” *Phys. Rev. B* **102**, 195401 (2020).
- [32] B. Roy, “Higher-order topological superconductors in \mathcal{P} -, \mathcal{T} -odd quadrupolar dirac materials,” *Phys. Rev. B* **101**, 220506 (2020).
- [33] S.-B. Zhang, W. B. Rui, A. Calzona, S.-J. Choi, A. P. Schnyder, and B. Trauzettel, “Topological and holonomic quantum computation based on second-order topological superconductors,” *Phys. Rev. Research* **2**, 043025 (2020).
- [34] M. Kheirkhah, Z. Yan, and F. Marsiglio, “Vortex-line topology in iron-based superconductors with and without second-order topology,” *Phys. Rev. B* **103**, L140502 (2021).
- [35] Z. Yan, “Higher-order topological odd-parity superconductors,” *Phys. Rev. Lett.* **123**, 177001 (2019).
- [36] J. Ahn and B.-J. Yang, “Higher-order topological superconductivity of spin-polarized fermions,” *Phys. Rev. Research* **2**, 012060 (2020).
- [37] X.-J. Luo, X.-H. Pan, and X. Liu, “Higher-order topological superconductors based on weak topological insulators,” *Phys. Rev. B* **104**, 104510 (2021).
- [38] Q. Wang, C.-C. Liu, Y.-M. Lu, and F. Zhang, “High-temperature majorana corner states,” *Phys. Rev. Lett.* **121**, 186801 (2018).
- [39] A. K. Ghosh, T. Nag, and A. Saha, “Hierarchy of higher-order topological superconductors in three dimensions,” *Phys. Rev. B* **104**, 134508 (2021).
- [40] B. Roy and V. Jurićić, “Mixed-parity octupolar pairing and corner majorana modes in three dimensions,” *Phys. Rev. B* **104**, L180503 (2021).
- [41] R. W. Bomantara, L. Zhou, J. Pan, and J. Gong, “Coupled-wire construction of static and floquet second-order topological insulators,” *Phys. Rev. B* **99**, 045441 (2019).
- [42] T. Nag, V. Jurićić, and B. Roy, “Out of equilibrium higher-order topological insulator: Floquet engineering and quench dynamics,” *Phys. Rev. Research* **1**, 032045 (2019).
- [43] Y. Peng and G. Refael, “Floquet second-order topological insulators from nonsymmorphic space-time symmetries,” *Phys. Rev. Lett.* **123**, 016806 (2019).
- [44] R. Seshadri, A. Dutta, and D. Sen, “Generating a second-order topological insulator with multiple corner states by periodic driving,” *Phys. Rev. B* **100**, 115403 (2019).
- [45] M. Rodriguez-Vega, A. Kumar, and B. Seradjeh, “Higher-order floquet topological phases with corner and bulk bound states,” *Phys. Rev. B* **100**, 085138 (2019).
- [46] A. K. Ghosh, G. C. Paul, and A. Saha, “Higher order topological insulator via periodic driving,” *Phys. Rev. B* **101**, 235403 (2020).
- [47] B. Huang and W. V. Liu, “Floquet higher-order topological insulators with anomalous dynamical polarization,” *Phys. Rev. Lett.* **124**, 216601 (2020).
- [48] H. Hu, B. Huang, E. Zhao, and W. V. Liu, “Dynamical

- singularities of floquet higher-order topological insulators," *Phys. Rev. Lett.* **124**, 057001 (2020).
- [49] Y. Peng, "Floquet higher-order topological insulators and superconductors with space-time symmetries," *Phys. Rev. Research* **2**, 013124 (2020).
- [50] T. Nag, V. Jurićić, and B. Roy, "Hierarchy of higher-order floquet topological phases in three dimensions," *Phys. Rev. B* **103**, 115308 (2021).
- [51] R.-X. Zhang and Z.-C. Yang, "Tunable fragile topology in floquet systems," *Phys. Rev. B* **103**, L121115 (2021).
- [52] R. V. Bhat and S. Bera, "Out of equilibrium chiral higher order topological insulator on a π -flux square lattice," *J. Phys. Condens. Matter* **33**, 164005 (2021).
- [53] W. Zhu, Y. D. Chong, and J. Gong, "Floquet higher-order topological insulator in a periodically driven bipartite lattice," *Phys. Rev. B* **103**, L041402 (2021).
- [54] J. Yu, R.-X. Zhang, and Z.-D. Song, "Dynamical symmetry indicators for floquet crystals," *Nature Communications* **12**, 5985 (2021).
- [55] D. Vu, "Dynamic bulk-boundary correspondence for anomalous floquet topology," *Phys. Rev. B* **105**, 064304 (2022).
- [56] A. K. Ghosh, T. Nag, and A. Saha, "Systematic generation of the cascade of anomalous dynamical first- and higher-order modes in floquet topological insulators," *Phys. Rev. B* **105**, 115418 (2022).
- [57] X.-L. Du, R. Chen, R. Wang, and D.-H. Xu, "Weyl nodes with higher-order topology in an optically driven nodal-line semimetal," *Phys. Rev. B* **105**, L081102 (2022).
- [58] Z. Ning, B. Fu, D.-H. Xu, and R. Wang, "Tailoring quadrupole topological insulators with periodic driving and disorder," (2022), [arXiv:2201.02414](https://arxiv.org/abs/2201.02414).
- [59] K. Plekhanov, M. Thakurathi, D. Loss, and J. Klinovaja, "Floquet second-order topological superconductor driven via ferromagnetic resonance," *Phys. Rev. Research* **1**, 032013 (2019).
- [60] R. W. Bomantara and J. Gong, "Measurement-only quantum computation with floquet majorana corner modes," *Phys. Rev. B* **101**, 085401 (2020).
- [61] R. W. Bomantara, "Time-induced second-order topological superconductors," *Phys. Rev. Research* **2**, 033495 (2020).
- [62] A. K. Ghosh, T. Nag, and A. Saha, "Floquet generation of a second-order topological superconductor," *Phys. Rev. B* **103**, 045424 (2021).
- [63] A. K. Ghosh, T. Nag, and A. Saha, "Floquet second order topological superconductor based on unconventional pairing," *Phys. Rev. B* **103**, 085413 (2021).
- [64] D. Vu, R.-X. Zhang, Z.-C. Yang, and S. Das Sarma, "Superconductors with anomalous floquet higher-order topology," *Phys. Rev. B* **104**, L140502 (2021).
- [65] A. K. Ghosh, T. Nag, and A. Saha, "Dynamical construction of quadrupolar and octupolar topological superconductors," *Phys. Rev. B* **105**, 155406 (2022).
- [66] N. Parappurath, F. Alpeggiani, L. Kuipers, and E. Verhagen, "Direct observation of topological edge states in silicon photonic crystals: Spin, dispersion, and chiral routing," *Science Advances* **6**, eaaw4137 (2020).
- [67] Y. Yang, Z. Gao, H. Xue, L. Zhang, M. He, Z. Yang, R. Singh, Y. Chong, B. Zhang, and H. Chen, "Realization of a three-dimensional photonic topological insulator," *Nature* **565**, 622–626 (2019).
- [68] S. Malzard, C. Poli, and H. Schomerus, "Topologically protected defect states in open photonic systems with non-hermitian charge-conjugation and parity-time symmetry," *Phys. Rev. Lett.* **115**, 200402 (2015).
- [69] A. Regensburger, C. Bersch, M.-A. Miri, G. Onishchukov, D. N. Christodoulides, and U. Peschel, "Parity-time synthetic photonic lattices," *Nature* **488**, 167–171 (2012).
- [70] R. El-Ganainy, K. G. Makris, M. Khajavikhan, Z. H. Musslimani, S. Rotter, and D. N. Christodoulides, "Non-hermitian physics and pt symmetry," *Nature Physics* **14**, 11–19 (2018).
- [71] M. M. Denner, A. Skurativska, F. Schindler, M. H. Fischer, R. Thomale, T. Bzdušek, and T. Neupert, "Exceptional topological insulators," *Nature Communications* **12**, 5681 (2021).
- [72] Z. H. Musslimani, K. G. Makris, R. El-Ganainy, and D. N. Christodoulides, "Optical solitons in \mathcal{PT} periodic potentials," *Phys. Rev. Lett.* **100**, 030402 (2008).
- [73] K. G. Makris, R. El-Ganainy, D. N. Christodoulides, and Z. H. Musslimani, "Beam dynamics in \mathcal{PT} symmetric optical lattices," *Phys. Rev. Lett.* **100**, 103904 (2008).
- [74] E. J. Bergholtz and J. C. Budich, "Non-hermitian weyl physics in topological insulator ferromagnet junctions," *Phys. Rev. Research* **1**, 012003 (2019).
- [75] K. Yang, S. C. Morampudi, and E. J. Bergholtz, "Exceptional spin liquids from couplings to the environment," *Phys. Rev. Lett.* **126**, 077201 (2021).
- [76] V. Kozii and L. Fu, "Non-hermitian topological theory of finite-lifetime quasiparticles: prediction of bulk fermi arc due to exceptional point," [arXiv:1708.05841](https://arxiv.org/abs/1708.05841).
- [77] T. Yoshida, R. Peters, and N. Kawakami, "Non-hermitian perspective of the band structure in heavy-fermion systems," *Phys. Rev. B* **98**, 035141 (2018).
- [78] H. Shen and L. Fu, "Quantum oscillation from in-gap states and a non-hermitian landau level problem," *Phys. Rev. Lett.* **121**, 026403 (2018).
- [79] S. Yao, F. Song, and Z. Wang, "Non-hermitian chern bands," *Phys. Rev. Lett.* **121**, 136802 (2018).
- [80] K. Kawabata, K. Shiozaki, M. Ueda, and M. Sato, "Symmetry and topology in non-hermitian physics," *Phys. Rev. X* **9**, 041015 (2019).
- [81] E. J. Bergholtz, J. C. Budich, and F. K. Kunst, "Exceptional topology of non-hermitian systems," *Rev. Mod. Phys.* **93**, 015005 (2021).
- [82] K. Sone, Y. Ashida, and T. Sagawa, "Exceptional non-hermitian topological edge mode and its application to active matter," *Nature Communications* **11**, 5745 (2020).
- [83] C. M. Bender, "Making sense of non-hermitian hamiltonians," *Rep. Prog. Phys.* **70**, 947–1018 (2007).
- [84] W. D. Heiss, "The physics of exceptional points," *J. Phys. A: Math. Theor.* **45**, 444016 (2012).
- [85] S. Yao and Z. Wang, "Edge states and topological invariants of non-hermitian systems," *Phys. Rev. Lett.* **121**, 086803 (2018).
- [86] F. K. Kunst, E. Edvardsson, J. C. Budich, and E. J. Bergholtz, "Biorthogonal bulk-boundary correspondence in non-hermitian systems," *Phys. Rev. Lett.* **121**, 026808 (2018).
- [87] T. Helbig, T. Hofmann, S. Imhof, M. Abdelghany, T. Kiessling, L. W. Molenkamp, C. H. Lee, A. Szameit, M. Greiter, and R. Thomale, "Generalized bulk-boundary correspondence in non-hermitian topoelectri-

- cal circuits,” *Nature Physics* **16**, 747–750 (2020).
- [88] D. S. Borgnia, A. J. Kruchkov, and R.-J. Slager, “Non-hermitian boundary modes and topology,” *Phys. Rev. Lett.* **124**, 056802 (2020).
- [89] R. Koch and J. C. Budich, “Bulk-boundary correspondence in non-hermitian systems: stability analysis for generalized boundary conditions,” *The European Physical Journal D* **74**, 70 (2020).
- [90] H.-G. Zirnstein, G. Refael, and B. Rosenow, “Bulk-boundary correspondence for non-hermitian hamiltonians via green functions,” *Phys. Rev. Lett.* **126**, 216407 (2021).
- [91] Y. Takane, “Bulk-boundary correspondence in a non-hermitian chern insulator,” *Journal of the Physical Society of Japan* **90**, 033704 (2021).
- [92] K. Zhang, Z. Yang, and C. Fang, “Correspondence between winding numbers and skin modes in non-hermitian systems,” *Phys. Rev. Lett.* **125**, 126402 (2020).
- [93] Z. Gong, Y. Ashida, K. Kawabata, K. Takasan, S. Higashikawa, and M. Ueda, “Topological phases of non-hermitian systems,” *Phys. Rev. X* **8**, 031079 (2018).
- [94] C. Yin, H. Jiang, L. Li, R. Lü, and S. Chen, “Geometrical meaning of winding number and its characterization of topological phases in one-dimensional chiral non-hermitian systems,” *Phys. Rev. A* **97**, 052115 (2018).
- [95] T. Liu, Y.-R. Zhang, Q. Ai, Z. Gong, K. Kawabata, M. Ueda, and F. Nori, “Second-order topological phases in non-hermitian systems,” *Phys. Rev. Lett.* **122**, 076801 (2019).
- [96] X.-W. Luo and C. Zhang, “Higher-order topological corner states induced by gain and loss,” *Phys. Rev. Lett.* **123**, 073601 (2019).
- [97] E. Edvardsson, F. K. Kunst, and E. J. Bergholtz, “Non-hermitian extensions of higher-order topological phases and their biorthogonal bulk-boundary correspondence,” *Phys. Rev. B* **99**, 081302 (2019).
- [98] Z. Zhang, M. Rosendo López, Y. Cheng, X. Liu, and J. Christensen, “Non-hermitian sonic second-order topological insulator,” *Phys. Rev. Lett.* **122**, 195501 (2019).
- [99] Y.-J. Wu, C.-C. Liu, and J. Hou, “Wannier-type photonic higher-order topological corner states induced solely by gain and loss,” *Phys. Rev. A* **101**, 043833 (2020).
- [100] R. Okugawa, R. Takahashi, and K. Yokomizo, “Second-order topological non-hermitian skin effects,” *Phys. Rev. B* **102**, 241202 (2020).
- [101] R. Okugawa, R. Takahashi, and K. Yokomizo, “Non-hermitian band topology with generalized inversion symmetry,” *Phys. Rev. B* **103**, 205205 (2021).
- [102] K. Shiozaki and S. Ono, “Symmetry indicator in non-hermitian systems,” *Phys. Rev. B* **104**, 035424 (2021).
- [103] Y. Yu, M. Jung, and G. Shvets, “Zero-energy corner states in a non-hermitian quadrupole insulator,” *Phys. Rev. B* **103**, L041102 (2021).
- [104] N. Okuma and M. Sato, “Topological phase transition driven by infinitesimal instability: Majorana fermions in non-hermitian spintronics,” *Phys. Rev. Lett.* **123**, 097701 (2019).
- [105] S. Lieu, “Non-hermitian majorana modes protect degenerate steady states,” *Phys. Rev. B* **100**, 085110 (2019).
- [106] J. Avila, F. Peñaranda, E. Prada, P. San-Jose, and R. Aguado, “Non-hermitian topology as a unifying framework for the andreev versus majorana states controversy,” *Communications Physics* **2**, 133 (2019).
- [107] X.-M. Zhao, C.-X. Guo, M.-L. Yang, H. Wang, W.-M. Liu, and S.-P. Kou, “Anomalous non-abelian statistics for non-hermitian generalization of majorana zero modes,” *Phys. Rev. B* **104**, 214502 (2021).
- [108] Z.-H. Wang, F. Xu, L. Li, D.-H. Xu, W.-Q. Chen, and B. Wang, “Majorana polarization in non-hermitian topological superconductors,” *Phys. Rev. B* **103**, 134507 (2021).
- [109] H. Liu, M. Lu, Y. Wu, J. Liu, and X. C. Xie, “Non-hermiticity stabilized majorana zero modes in semiconductor-superconductor nanowires,” (2021), [arXiv:2111.11731](https://arxiv.org/abs/2111.11731).
- [110] H. Shen, B. Zhen, and L. Fu, “Topological band theory for non-hermitian hamiltonians,” *Phys. Rev. Lett.* **120**, 146402 (2018).
- [111] K. Esaki, M. Sato, K. Hasebe, and M. Kohmoto, “Edge states and topological phases in non-hermitian systems,” *Phys. Rev. B* **84**, 205128 (2011).
- [112] W. Chen, M. Legner, A. Rüegg, and M. Sigrist, “Correlation length, universality classes, and scaling laws associated with topological phase transitions,” *Phys. Rev. B* **95**, 075116 (2017).
- [113] R. Arouca, C. H. Lee, and C. Morais Smith, “Unconventional scaling at non-hermitian critical points,” *Phys. Rev. B* **102**, 245145 (2020).
- [114] H. Miyake, G. A. Siviloglou, C. J. Kennedy, W. C. Burton, and W. Ketterle, “Realizing the harper hamiltonian with laser-assisted tunneling in optical lattices,” *Phys. Rev. Lett.* **111**, 185302 (2013).
- [115] D. McKay and B. DeMarco, “Cooling in strongly correlated optical lattices: prospects and challenges,” *Reports on Progress in Physics* **74**, 054401 (2011).
- [116] J. Bezanson, A. Edelman, S. Karpinski, and V. B. Shah, “Julia: A fresh approach to numerical computing,” *SIAM review* **59**, 65–98 (2017).